JOURNAL OF OPTOELECTRONICS AND ADVANCED MATERIALS Vol. 10, No. 7, July 2008, p. 1700 - 1703

Pseudogap and magnetic incommensurability in the Hubbard model

A. SHERMAN,* M. SCHREIBER[a]
Institute of Physics, University of Tartu, Riia 142, 51014 Tartu, Estonia
[a]*Institut für Physik, Technische Universität, 09107 Chemnitz, Germany*

The electron energy spectrum and the magnetic susceptibility of the two-dimensional repulsive Hubbard model are investigated using the diagram technique for the case of strong correlations. In this technique a power series in the hopping constant is used. Obtained results reproduce adequately available data of Monte Carlo simulations. With departure from half-filling *x* our calculated spectrum demonstrates a pseudogap near the Fermi level and an excitation band with the properties of the spin-polaron band of the *t-J* model. The low-frequency magnetic susceptibility becomes incommensurate and the incommensurability parameter grows with *x*. The value of the incommensurability parameter, its dependence on the transfer frequency and on *x* resemble experimental results in lanthanum cuprates.

(Received April 1, 2008; accepted June 30, 2008)

Keywords : Hubbard model, Energy spectrum, Pseudogap, Magnetic susceptibility, Magnetic incommensurability

The discovery of high-T_C superconductors and heavy-fermion compounds has revived interest in strongly correlated electron systems. One of the simplest and still realistic models in this field is the one-band Hubbard model [1] two-dimensional version of which has been extensively studied in connection with the cuprate perovskite superconductors. The Hamiltonian of the model reads

$$H = \sum_{\mathbf{ll'}\sigma} \mathbf{t_{ll'}} \mathbf{a}^{\dagger}_{\mathbf{l}\sigma} \mathbf{a}_{\mathbf{l'}\sigma} + \frac{\mathbf{U}}{\mathbf{2}} \sum_{\mathbf{l}\sigma} \mathbf{n}_{\mathbf{l}\sigma} \mathbf{n}_{\mathbf{l},-\sigma}, \quad (1)$$

where $a^{\dagger}_{\mathbf{l}\sigma}$ and $a_{\mathbf{l}\sigma}$ are the electron creation and annihilation operators, **l** labels sites of the square plane lattice, σ=±1 is the spin projection, $t_{\mathbf{ll'}}$ and *U* are hopping and on-site repulsion constants, and $n_{\mathbf{l}\sigma} = a^{\dagger}_{\mathbf{l}\sigma} a_{\mathbf{l}\sigma}$.

The idea of strong-coupling diagram technique for this model traces back to early works by J. Hubbard [1] and is based on the fact that if the Coulomb repulsion dominates, $U \geq |t_{11'}|$, it is reasonable to treat the kinetic energy in the framework of a perturbation theory. In the diagram technique of Refs. [2, 3] this expansion for Green's function is expressed in terms of site cumulants of electron creation and annihilation operators. Cumulants of the first two orders read

$$K_1(\tau',\tau) = \left\langle T\bar{a}_{\mathbf{l}\sigma}(\tau') a_{\mathbf{l}\sigma}(\tau) \right\rangle_0,$$

$$K_2(\tau'\sigma, \tau\sigma, \tau'_1\sigma_1, \tau_1\sigma_1) = \left\langle T\bar{a}_{\mathbf{l}\sigma}(\tau') a_{\mathbf{l}\sigma}(\tau) \bar{a}_{\mathbf{l}\sigma_1}(\tau'_1) a_{\mathbf{l}\sigma_1}(\sigma_1) \right\rangle_0 \quad (2)$$

$$- K_1(\tau',\tau) K_1(\tau'_1,\tau_1) + K_1(\tau',\tau_1) K_1(\tau'_1,\tau) d_{\sigma\sigma_1},$$

where *T* is the time-ordering operator which arranges other operators from right to left in ascending order of times τ, the subscript 0 of the angular brackets indicates that the statistical averaging and time dependencies of the operators

$$\bar{a}_{\mathbf{l}\sigma}(t) = \exp(H_{\mathbf{l}} t) a^{\dagger}_{\mathbf{l}\sigma} \exp(-H_{\mathbf{l}} t)$$

are determined by the site Hamiltonian

$$H_{\mathbf{l}} = \sum_s \left[(U/2) n_{\mathbf{l}\sigma} n_{\mathbf{l},-\sigma} - \mu n_{\mathbf{l}\sigma} \right]$$

with the chemical potential μ. All operators in the cumulants belong to the same lattice site. Due to the translational symmetry the cumulants do not depend on the site position.

Let us consider the application of this diagram technique to the electron Green's function

$$G(1'\tau', 1\tau) = \left\langle T\bar{a}_{\mathbf{l'}\sigma}(\tau') a_{\mathbf{l}\sigma}(\tau) \right\rangle, \quad (3)$$

where the statistical averaging and time dependencies of operators are determined by the Hamiltonian $H = H - \mu \sum_{\mathbf{l}\sigma} \mathbf{n}_{\mathbf{l}\sigma}$. It is convenient to introduce the notion of an irreducible diagram which cannot be divided into two parts by cutting a hopping line. The irreducible diagrams of the first four orders which contribute to Green's function (3) are shown in Fig. 1 with their signs and prefactors.

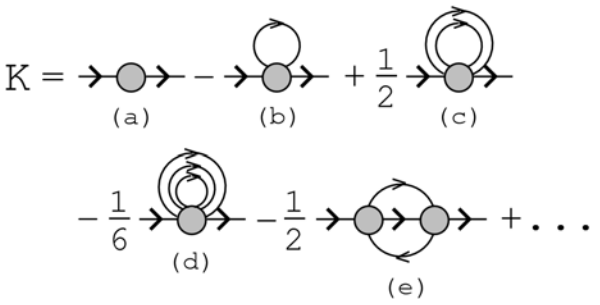

Fig. 1. Irreducible diagrams of the first four orders of the expansion in powers of t_k.

In this figure, circles are the cumulants which orders are determined by the number of incoming or outgoing lines. These lines symbolize hopping between sites caused by the kinetic term of Hamiltonian (1). The bare hopping line corresponds to the multiplier $t_{\mathbf{k}}$ which is a Fourier transform of the hopping constants $t_{\mathbf{ll}'}$ with the wave vector **k**. The diagram technique admits partial summation in which irreducible diagrams are inserted in the internal hopping lines of diagrams in Fig. 1. As a consequence the bare hopping $t_{\mathbf{k}}$ is substituted by the renormalized one,

$$\Theta(\mathbf{k},n)=t_{\mathbf{k}}+t_{\mathbf{k}}^2 G(\mathbf{k},n), \qquad (4)$$

where the integer n stands for the fermion Matsubara frequency $\omega_n=(2n+1)\pi T$ with the temperature T and $G(\mathbf{k},n)$ is the respective Fourier transform of Green's function (3). This function satisfies the Larkin equation

$$G(\mathbf{k},n)=\frac{K(\mathbf{k},n)}{1-t_{\mathbf{k}}K(\mathbf{k},n)}, \qquad (5)$$

where $K(\mathrm{k},n)$ is the sum of all irreducible diagrams.

In our calculations this total sum of irreducible diagrams was substituted by the contribution of the diagrams (a), (b), and (e) in Fig. 1. Ignoring the diagrams (c) and (d) was motivated by the fact that for $t_{\mathbf{ll}}=0$ their contributions start from terms of the fourth and sixth orders in $t_{\mathbf{k}}$, respectively, while the lowest-order term of the diagram (e) is of the third order. Besides, the diagrams (c) and (d) give contributions of the same local type as the diagram (b). Due to their higher order the contributions are expected to give small corrections to the diagram (b). For Green's functions in the renormalized hopping lines (4) we used the Hubbard-I approximation. It is obtained if in Eq. (5) the diagram (a) with the first-order cumulant K_1, Eq. (2), is used instead of the total sum of irreducible diagrams [2, 3]. In this approach, the solution obtained after the transition from imaginary to real frequencies has a flaw – a negative spectral weight near $\omega=-\mu$ and $U-\mu$ [2, 3]. To overcome this difficulty for the analytic continuation to the real frequency axis we used a Padé approximant of the considered Green's function, applying the procedure described in Ref. [4]. The reason for such an approach is the fact that domains of analyticity of Padé approximants and approximated functions are generally different. In our case this procedure did allow us to remedy the mentioned flaw.

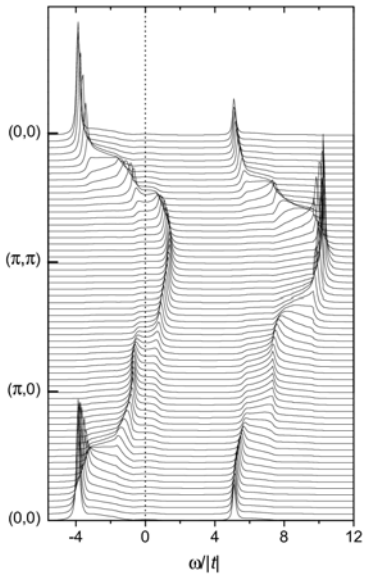

Fig. 2. The spectral function $A(\mathbf{k},\omega)$ calculated for momenta along the symmetry lines of the square Brillouin zone in a 40×40 lattice for $t=-U/8$, $T=0.001U$, and $x=0.12$.

The spectral function

$$A(k,\omega)=-\pi^{-1}\,\mathrm{Im}\,G(k,w)$$

calculated in this approach reproduces the key features of spectra obtained by Monte Carlo simulations [5] and cluster methods [6]. In particular, at half-filling, $\mu=U/2$, $\bar{n}=\langle n_{1\sigma}\rangle=1$, the spectrum has a four-band structure – each of the Hubbard bands splits into two subbands. It follows from our calculations that this splitting occurs due to two pronounced minima in $\mathrm{Im}K(\mathbf{k},\omega)$. Maxima in the spectral function arise at frequencies which satisfy the condition $1-t_{\mathbf{k}}\,\mathrm{Re}\,K(\mathbf{k},w)=0$ and are located on either side of the minima of $\mathrm{Im}K(\mathbf{k},\omega)$. It looks like each of the minima splits the Hubbard band into two subbands. The four-band structure is partly retained on departure from half-filling.

An example of the obtained spectral function is shown in Fig. 2. Hereafter we consider the case where only the constant t for hopping between nearest neighbor sites is nonzero. The considered model possesses the electron-hole symmetry. Therefore in the following discussion we shall restrict our consideration to the case $\bar{n}\le 1$ and set

x=1$-\bar{n}$. In the spectrum in Fig. 2, the suppression of the spectral intensity near the Fermi level is noteworthy. This suppression creates a pseudogap which owes its origin to strong electron correlations. Recently spectra with analogous pseudogaps were also obtained by cluster methods [6]. In our calculations the pseudogap appears at $x\approx0.06$ and disappears at $x\approx0.2$. Analogous behavior of the pseudogap was found in the photoemission of cuprates [7] and in the related *t*-*J* model [8].

With departure from half-filling, already at small x a new dispersive band appears in the spectrum. In Fig. 2 the respective maxima are seen below the Fermi level. The dispersion of the band is much larger in the direction (0,0)–(π,π) than along (π,0)–(0,π) where the maximum energies of the band are located. For small x the width of the band is approximately equal to $2J$ where $J=4t^2/U$ is the superexchange constant. The bandwidth decreases with increasing x. In these properties the band resembles the spin-polaron band of the *t*-*J* model [9].

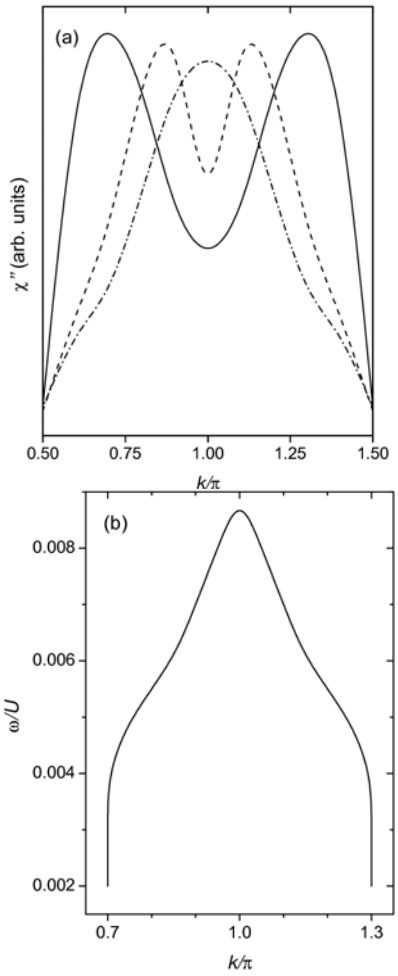

Fig. 3. (a) The momentum dependence of $\chi''(\mathbf{k}\omega)$ for $\mathbf{k}=(k,k)$, $t=-U/8$, $T=0.06U$, $\omega=0.002U$ and $\bar{n}=1$ (dash-dotted line), $\bar{n}\approx0.94$ (dashed line), and $\bar{n}\approx0.88$ (solid line). (b) The dispersion of maxima in $\chi''(\mathbf{k}\omega)$ for $t=-U/8$, $T=0.06U$, and $\bar{n}\approx0.88$.

Now let us consider the application of the diagram technique discussed above for calculating the spin Green's function

$$D(1'\tau',1,\tau)=Ts_{\mathbf{l}}^{\sigma}(\tau')s_{\mathbf{l}}^{-\sigma}(\tau), \tag{6}$$

where $s_{\mathbf{l}}^{\sigma}=a_{\mathbf{l}\sigma}^{\dagger}a_{\mathbf{l},-\sigma}$ is the spin operator. Using this technique it can be shown that the function satisfies the equation

$$D(p)=-N^{-1}T\sum_{p_1}G(p_1)G(p+p_1)+$$
$$N^{-2}T^2\sum_{p_1p_2}\Pi(p_1)\Pi(p_2)\Pi(p+p_1)\Pi(p+p_2)$$
$$\times\Gamma(p_1,p+p_1,p+p_2,p_2), \tag{7}$$

where the combined indices $p=(\mathbf{k},i\omega_\nu)$ and $p_j=(\mathbf{k}_j,i\omega_{n_j})$ were introduced, $\omega_\nu=2\nu\pi T$ is the boson Matsubara frequency, $\Pi(\mathbf{k},n)=\Theta(\mathbf{k},n)/t_{\mathbf{k}}$, N is the number of sites, and $\Gamma(p_1,p+p_1,p+p_2,p_2)$ is the sum of all four-leg diagrams. In such a diagram, starting from any leg, i.e. an external end of the diagram, one can reach any other leg moving along the hopping lines and cumulants. Among the four-leg diagrams a subset of irreducible diagrams $\gamma(p_1,p+p_1,p+p_2,p_2)$ can be separated. These latter diagrams cannot be divided into two disconnected parts by cutting two hopping lines. The sum of all four-leg diagrams satisfies the Bethe-Salpeter equation

$$\Gamma(p_1,p+p_1,p+p_2,p_2)=\gamma(p_1,p+p_1,p+p_2,p_2)$$
$$-N^{-1}T\sum_{p_3}\gamma(p_1,p+p_1,p+p_3,p_3)\Theta(p_3)\Theta(p+p_3)$$
$$\times\Gamma(p_3,p+p_3,p+p_2,p_2). \tag{8}$$

In the following calculations we simplified the general equations (7) and (8) by using bare hopping lines instead of the renormalized ones and by employing the lowest-order irreducible four-leg diagram instead of $\gamma(p_1,p+p_1,p+p_2,p_2)$. This four-leg diagram is described by the second-order cumulant K_2, Eq. (2). In this approximation the Bethe-Salpeter equation (8) can be solved exactly.

We found that at half-filling our calculated temperature dependence of the zero-frequency magnetic susceptibility reproduces adequately key features of results of Monte Carlo simulations [10]. In particular, the uniform susceptibility tends to a finite value for vanishing temperature as it must. The staggered susceptibility diverges with decreasing temperature which signals the establishment of the long-range antiferromagnetic order. The transition temperature is finite which indicates the violation of the Mermin-Wagner theorem [11]. However,

the transition temperature is always lower than the analogous temperature in the random phase approximation. Besides, the transition temperature decreases with decreasing the ratio $|t|/U$, i.e. the violation of the Mermin-Wagner theorem becomes less pronounced on enforcing the condition for which the approximation was developed. For small values of this ratio the calculated square of the site spin differs by less than 10% from the results of Monte Carlo simulations. Also in agreement with these results we found no evidence of ferromagnetic correlations in the considered range of electron concentrations $0.8 \bar{n} \leq 1$ for the repulsion parameters $8|t| \leq U \leq 16|t|$.

The imaginary part of the real-frequency susceptibility,

$$\chi''(k\omega) = \mathrm{Im}\, D(k, \omega + i\eta),\ \eta \to +0 \qquad (9)$$

is of special interest, because it determines the dynamic structure factor measured in neutron scattering experiments. The calculated momentum dependence of this susceptibility for a fixed transfer frequency is shown in Fig. 3 (a). Wave vectors were taken along the diagonal of the Brillouin zone. As seen from the figure, with departure from half-filling $\chi(\mathbf{k},\omega)$ becomes incommensurate – the momentum of its maximum deviates from (π,π). The incommensurability parameter, i.e. the distance between (π,π) and the wave vector of the susceptibility maximum, grows with x. As seen from Fig. 3 (b), for a fixed electron concentration the incommensurability parameter decreases with increasing ω and at some frequency the incommensurability disappears – the susceptibility appears to be peaked at the antiferromagnetic momentum.

This behavior of the susceptibility in the Hubbard model resembles the low-frequency incommensurate magnetic response observed by inelastic neutron scattering in lanthanum cuprates [12]. Also the value of the incommensurability parameter is close to that measured experimentally. The dispersion which is analogous to that shown in Fig. 3 (b) forms the lower part of the "sand-glass" dispersion found in these crystals. It should be emphasized that in the Hubbard model the magnetic incommensurability is a property of strong electron correlations. The similarity of the mentioned experimental and calculated results gives reason to consider these strong correlations as a possible mechanism of the low-frequency incommensurability observed in experiment. A similar mechanism was considered for the related t-J model in Ref. [13].

In summary, the strong-coupling diagram technique allowed us to reveal several essential features of the Hubbard model. Among them are the four-band structure of the electron spectrum near half-filling, the pseudogap and the analog of the spin-polaron band which appear near the Fermi level at some departure from half-filling. We found also the low-frequency incommensurability in the magnetic response of this model with properties which are similar to those observed in lanthanum cuprates.

Acknowledgments

This work was partially supported by the ETF grant No. 6918 and by the DFG.

References

[1] J. Hubbard, Proc. R. Soc. London, Ser. A **296**, 82 (1966).
[2] M. I. Vladimir, V. A. Moskalenko, Teor. Mat. Fiz. **82**, 428 (1990) [Theor. Math. Phys. **82**, 301 (1990)]; W. Metzner, Phys. Rev. B **43**, 8549 (1991).
[3] A. Sherman, Phys. Rev. B **73**, 155105 (2006); **74**, 035104 (2006).
[4] H. J. Vidberg, J. W. Serene, J. Low Temp. Phys. **29**, 179 (1977).
[5] A. Moreo, S. Haas, A. W. Sandvik, and E. Dagotto, Phys. Rev. B **51**, 12045 (1995); C. Gröber, R. Eder, W. Hanke, Phys. Rev. B **62**, 4336 (2000).
[6] T. Maier, M. Jarrell, T. Pruschke, and M. H. Hettler, Rev. Modern Phys. **77**, 1027 (2005).
[7] A. Damascelli, Z. Hussain, and Z.-X. Shen, Rev. Modern Phys. **75**, 473 (2003).
[8] A. Sherman, M. Schreiber, Phys. Rev. B **55**, R712 (1997).
[9] Yu. A. Izyumov, Usp. Fiz. Nauk **167**, 465 (1997) [Phys.-Usp. (Russia) **40**, 445 (1997)].
[10] J. E. Hirsch, Phys. Rev. B **31**, 4403 (1985).
[11] N. D. Mermin, H. Wagner, Phys. Rev. Lett. **17**, 1133 (1966).
[12] K. Yamada, C. H. Lee, K. Kurahashi, J. Wada, S. Wakimoto, S. Ueki, H. Kimura, Y. Endoh, S. Hosoya, G. Shirane, R. J. Birgeneau, M. Greven, M. A. Kastner, Y. J. Kim, Phys. Rev. B **57**, 6165 (1998).
[13] A. Sherman, M. Schreiber, Phys. Rev. B **69**, 100505(R) (2004); Int. J. Modern Phys. B **19**, 2145 (2005); **21**, 669 (2007).

*Corresponding author: alexei@fi.tartu.ee